Large Spatial Model: End-to-end Unposed Images to Semantic 3D

Zhiwen Fan[1,2†*], **Jian Zhang**[3*], **Wenyan Cong**[1], **Peihao Wang**[1], **Renjie Li**[4], **Kairun Wen**[3], **Shijie Zhou**[5], **Achuta Kadambi**[5], **Zhangyang Wang**[1], **Danfei Xu**[2,6], **Boris Ivanovic**[2‡], **Marco Pavone**[2,7], **Yue Wang**[2,8]
[†] Project Lead [‡] Corresponding Author

[1]UT Austin [2]NVIDIA Research [3]Xiamen University
[4]TAMU [5]UCLA [6]GaTech [7]Stanford University [8]USC

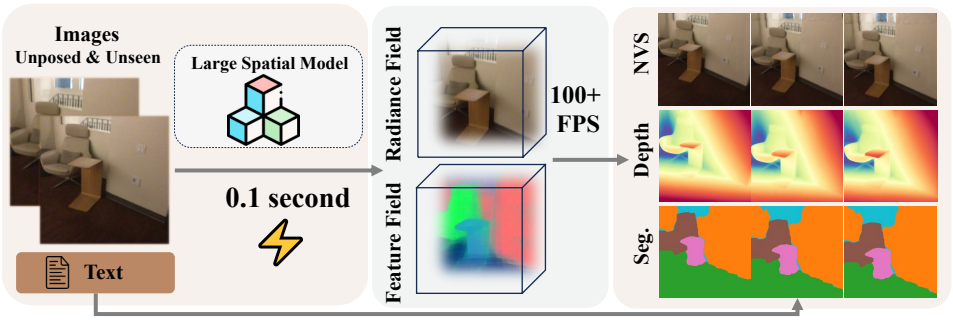

Figure 1: **Large Spatial Model** takes two unposed images as input, and reconstructs the explicit radiance field, encompassing geometry, appearance, and semantics in real-time, facilitating view synthesis, depth prediction, and open-vocabulary segmentation.

Abstract

A classical problem in computer vision is to reconstruct and understand the 3D structure from a limited number of images. Traditional approaches typically decompose this objective into multiple subtasks, involving several stages of complicated mapping among different data representations. For instance, dense reconstruction through Structure-from-Motion (SfM) first requires transforming a set of images into key points and optimizing the camera parameters before estimating structures. The subsequent 3D understanding relies on a an accurate sparse reconstruction and lengthy dense modeling before inputting into data- and task-specific neural networks. This paradigm can result in extensive processing times and engineering efforts. In this work, we introduce the Large Spatial Model (**LSM**) that directly processes unposed RGB images into semantic radiance fields. This new model simultaneously estimate geometry, appearance, and semantics all in a single feed-forward pass, and able to synthesize versatile label maps by interacting using language at novel views. LSM is general where generic Transformer-based frameworks are applied that integrates global geometry by pixel-aligned point maps. To facilitate spatial attributes regression, we adopt local context aggregation with multi-scale fusion tailored for enhanced prediction accuracy in local details. Addressing the scarcity of labeled 3D semantic data and enhancing scene manipulation capabilities via natural language, we incorporate a well-trained 2D language-based segmentation model into a 3D consistent semantic feature field. An efficient decoder parameterizes a set of anisotropic Gaussians, enabling supervised end-to-end learning. Comprehensive experiments on various tasks demonstrate that LSM can unify multiple 3D vision tasks directly from unposed images. It also achieves both real-time semantic 3D reconstruction for the first time.

[*]Equal Contribution

Preprint. Under review.

1 Introduction

The computer vision community has devoted considerable effort to recovering and understanding 3D information (e.g., depth and semantics) from 2D sensory data (e.g. images). This process aims to derive 3D representations that encapsulate both geometric and semantic details from cheap and widely available 2D data, facilitating further interaction, reasoning and planning within 3D physical world Traditional approaches [1] tackle this by pipelining several distinct tasks: detecting, matching, and triangulating points for initial sparse reconstructions and the subsequent dense reconstruction, followed by the integration of specialized sub-modules for semantic 3D modeling. Recent developments in this domain have markedly proceed with more powerful representation using both sparse reconstruction [1], and subsequent dense 3D modeling using either Multi-View Stereo(MVS) [2, 3], Neural Radiance Field [4], and Gaussian Splatting [5], This trend influenced various industries, including autonomous driving [6], robotics [7], digital twins [8], and virtual/augmented reality (VR/AR) [9, 10]. Due to the complexity of inferring 3D information from 2D images, previous methods have broken down the holistic task into distinct, manageable sub-problems. However, this strategy propagates errors from one stage to the next and downgrades the performance of subsequent tasks. For instance, the critical step of pre-computing camera poses—utilizing Structure from Motion [1]—has proven to be vulnerable and often fails in scenes covered by a sparse number of views or exhibiting low-textured surfaces [11]. Such inaccuracies in camera pose estimation can ultimately lead to imprecise interpretation of the 3D scene. Additionally, reasoning about and interacting with the environment would benefit from a comprehensive 3D understanding. Open-vocabulary methods, which perform semantic segmentation without relying on a fixed set of labels, provide notable flexibility in this regard. However, unlike single-image understanding, the absence of large-scale and diverse 3D scene data with accurate multi-view language annotations complicates the challenge. Efforts have been made to integrate 2D features into frameworks such as NeRF [4, 12] and 3D-GS [5, 13]. Yet, these methods, such as Feature-3DGS [13], typically require overfitting each 3D scene separately with extensive captured viewpoints and preprocessing of camera poses using Structure-from-Motion.

To overcome all above mentioned issues, we, for the first time, propose to unify all these 3D problems ranging from dense 3D reconstruction, open-vocabulary semantic segmentation, and novel-view synthesis from unposed and uncalibrated images using an end-to-end strategy. Specifically, we address all above challenges by utilizing a single Transformer-based model that learns the attributes of a 3D scene represented by a point-based semantic radiance field. Unlike previous works that either adapt epipolar Transformers [14, 15, 16] assuming known camera parameters or require hours of per-scene fitting [5, 13], we rely on a coarse-to-fine strategy to predict dense 3D geometry by pixel-aligned point maps, and future aggregate points into anisotropic Gaussians, through a feed-forward pass. Our method, the Large Spatial Model (LSM), begins by using a general Transformer architecture with cross-view attention [17] to construct the scene represented by pixel-aligned point maps at a normalized scale which facilitate the generalization across different data sources. Subsequently, LSM employs local context aggregation with multi-scale fusion, leveraging the semantic-rich ViT encoder to enhance point-based representations. Feed-forward 3D scene understanding using language is achieved through hierarchical cross-modal fusion, where features from a pre-trained 2D semantic model are fused into a consistent 3D feature field. By decoding using differentiable splatting, LSM can be supervised end-to-end under data-driven fashion and enables the rendering of various labels at any new viewpoint. LSM addresses multiple 3D vision tasks within a unified framework. LSM is efficient and capable of performing both scene-level 3D semantic reconstruction and rendering in real time without the extra step of computing camera parameters, we show an example scene in Figure 1.

Our contributions are summarized as follows:

- We propose a general and unified 3D representation and propose a end-to-end framework that solves dense 3D reconstruction, 3D language-based segmentation, and novel-view synthesis directly from unposed images in a single forward pass.
- Our approach leverages a generic Transformer architecture enhanced with cross-view attention to integrate multi-view cues for initial pixel-aligned multi-view geometry prediction, and hierarchical cross-model attention to propagate geometric rich encode feature and a well-trained semantic segmentation model for 3D understanding. By aggregating local context at the point-level, we achieve fine-grained feature integration for the prediction of anisotropic 3D Gaussians while enabling efficient splatting for RGB, depth and semantics.

- Our model efficiently executes multiple tasks simutaneously and is capable of performing real-time reconstruction and rendering on a single GPU. Experiments demonstrate that a unified representation of multiple 3d vision problems is scalable, while surpass many state-of-the art baselines that requires additional SfM step.

2 Related Works

End-to-end Image-to-3D 3D reconstruction is a long-standing research problem in computer vision, involving both appearance [18, 19, 4, 5] and geometry [20, 21, 22, 23]. Recent methods have emerged for predicting 3D geometry from a single RGB image by leveraging neural networks to learn strong 3D priors from large datasets. These approaches, inherently ill-posed without additional assumptions, address ambiguities effectively. They fall into three categories: the first relies on a single panorama as the global scene representation and utilizes novel view synthesis (NVS) techniques like NeRF [4] or 3DGS [5] to lift the 3D radiance field [24, 25]. The second uses class-level object priors to reconstruct shape, pose, and appearance from 2D images [26, 27, 28]. However, these methods struggle with objects from unseen categories. The third category, closer to our method, targets general scenes using established monocular depth estimation networks [29, 30, 31, 32] to generate pixel-aligned 3D point-clouds from depth maps and camera intrinsics. For instance, SynSin [33] renders new viewpoints from feature-augmented depth maps with known camera parameters. Methods without camera intrinsics rely on video frames' temporal consistency [34, 35, 36] or predict intrinsics directly for metric 3D reconstruction [37, 31], though their effectiveness is limited by depth estimate quality. However, existing generalizable NVS methods [16, 15], are typically limited to rendering target view colors, without the understanding of the 3D scene.

SfM and Differentiable Neural Representation Structure-from-Motion (SfM) techniques aim to jointly estimate camera poses and reconstruct sparse 3D structure from multiple views of a scene. The traditional pipeline involves a multi-stage process of descriptor extraction, correspondence estimation, and subsequent incremental bundle adjustment. Recently, the SfM pipeline has been continuously improved by integrating learning-based techniques. The success of these techniques has led to their widespread adoption, and existing differentiable neural representations are designed with the implicit assumption that the SfM techniques provide accurate poses in the wild. For example, NeRF [4] and its many successors (e.g. [38, 39]) utilize poses estimated offline with COLMAP [1, 40]. 3D Gaussian Splatting [5] directly leverages the 3D points provided by SfM as an initialization. Besides novel view synthesis, lifting features from 2D models to 3D space also gains popularity in multiple editing tasks [12, 13, 41].

Semantic 3D Modeling Segmentation 3D modeling involves both the segmentation of pre-computed 3D structures like voxel grids or point clouds [42, 43, 44, 45, 46], and the concurrent segmentation and reconstruction from 2D images [47, 48, 49]. Neural Radiance Fields (NeRFs) offer a unified representation to model a scene's photo-realistic appearance [38, 50, 4], geometry [51, 52, 53], and other spatially-varying properties [54, 55, 56] (e.g., semantics). Among them, Zhi et al. [54] first incorporated semantics into NeRF, demonstrating how 2D semantic segmentations, despite the noise, could be integrated into a coherent volumetric model to enhance accuracy and enable novel view synthesis of semantic masks. Following this, several studies have expanded upon this concept, for example, by incorporating instance modeling [57, 58, 59] or abstract visual features that allow for post-hoc semantic segmentation [12, 55].

3 Methods

Overview We illustrate the architecture for training LSM in Figure 2, where the input consists of stereo image pairs and associated camera poses in training $\{(\boldsymbol{I}_i \in \mathbb{R}^{H\times W\times 3}), (\boldsymbol{T}_i \in \mathbb{R}^{3\times 4})\}_{i=1}^{2}$, While in the inference stage, unposed images can be directly feed into the framework. The pixel-aligned geometry is predicted using a standard Transformer architecture [60] with cross-attention between input views and dense prediction heads are then employed to regress normalized point maps $\{\boldsymbol{D}_i \in \mathbb{R}^{H\times W\times 3}\}_{i=1}^{2}$ (Sec. 3.1). To enable fine-grained anisotropic 3D Gaussian regression to represent the 3D scene, and facilitate the lifting of generic feature fields from 2D pre-trained vision models, substraction-based attention with learnable positional encoding are applied in a local window to propagate features from neighboring points (Sec. 3.2), and thus amalgamate encoded features with rich semantics (Sec. 3.2) by lifting 2D pre-trained model (Sec. 3.3) at multi-scale. New views from

semantic radiance fields can be decoded using splatting [5] on the target poses(Sec. 3.4). During inference stage, normalized point maps can be directly predicted where the renderer take the camera parameters calculated based on point maps. Overview of our model is shown in Figure 2.

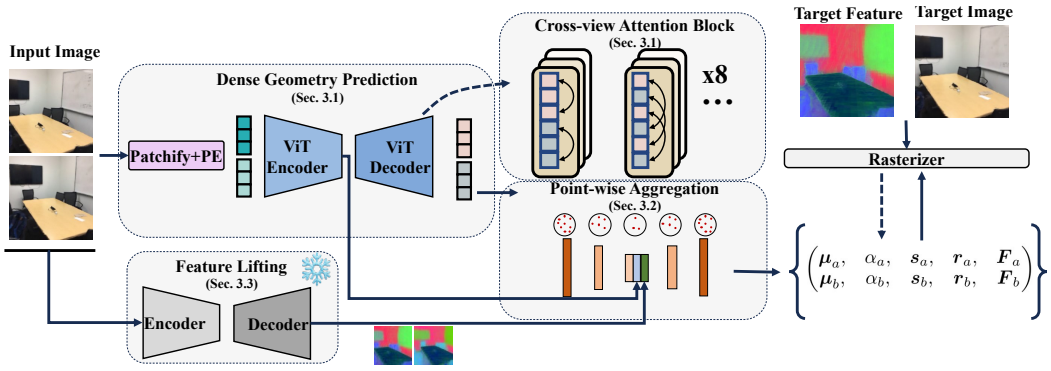

Figure 2: **Network Architecture.** Our method utilizes input images from which pixel-aligned point maps are regressed using a generic Transformer. A set of anitrosopic 3D Gaussians incorporating geometry, appearance, and semantics are then predicted employing another point-based Transformer that facilitates local context aggregation and hierarchical fusion. It is supervised end-to-end, minimizing the loss function through comparisons against ground truth and rasterized label maps on new views. During the inference stage, our approach is capable of predicting the scene representation without requiring camera parameters, enabling real-time semantic 3D reconstruction.

3.1 Dense Geometry Prediction

Instead of adopting a conventional Transformer with Epipolar attention—which can be inefficient as pixel-wise prediction requires hundreds of queries on sampled epipolar lines [14, 15]—we implement an encoder-decoder structure for directly regressing view-specific point maps at normalized scales. Cross-view attention is utilized to aggregate multi-view information efficiently.

Direct Regression of Normalized Depth Map We employ a Siamese ViT-based encoder [60] that processes stereo images using shared weights. It involves the patchification and tokenization of images, followed by the integration of sinusoidal positional embeddings.

To directly regress the pixel-aligned point maps from the unposed images, cross-view attention is also employed, enhancing the architecture's capacity to infer spatial relationships and propagate information between views—an approach that has proven effective in prior research [61, 17, 62]. The decoder block consists of interleaved self-attention for each view and cross-attention across views, which integrates tokens from both images. The inter-view decoder includes eight attention blocks, akin to those utilized in previous multi-view stereo (MVS) studies [62, 17]. These blocks generate tokenized features for a subsequent Dense Prediction Transformer head (DPT) [30], which estimates a pixel-wise point map in a normalized coordinate system:

$$\mathcal{L}_{\text{depth}} = \sum_{v \in \{1,2\}} \left\| \text{Norm}(\boldsymbol{D}_{v,1}) - \text{Norm}(\hat{\boldsymbol{D}}_{v,1}) \right\| \tag{1}$$

For a more detailed explanation of the loss function by normalizing and combining data from different sources.

3.2 Point-wise Feature Aggregation

Drawing inspiration from seminal works in neural radiance fields [4] and multi-view stereo [3], where coarse-to-fine stretegy is applied for high-quality radiance field and depth estimation. Here, we apply another Transformer worked on the point-level with hierarchical representation for finer point-based prediction.

Point-wise Attribute Prediction Rather than relying solely on a single network to represent the scene, we employ two Transformer-based networks optimized for distinct tasks: one for capturing "coarse" global geometry and another for "fine" local information aggregation. Initially, we

integrate stereo point maps, including color information for each point primitive, formulated as $\{\boldsymbol{p}_i = (x_i, y_i, z_i, r_i, g_i, b_i)\}_{i=1}^{N}$ to serve as input. Unlike tokenized image patches, point primitives provide unique geometric meanings within Euclidean space. Drawing from advancements in point cloud processing literature [63, 64, 65], we deploy a Transformer within a constrained window to perform point-wise aggregation, strategically highlighting essential features from adjacent primitives. Point-wise encoding and decoding, crucial for refining scene representation, involve a multi-scale aggregation across five levels.

After aggregating the point-wise features, we employ multiple Multilayer Perceptrons (MLPs) to regress the parameters, representing the 3D scene through a set of anisotropic Gaussians [5]. The parameters include the Gaussian centers $\boldsymbol{\mu}$, opacity α, scale factor $\boldsymbol{s}$, rotation $\boldsymbol{r}$, and Spherical Harmonics coefficients $\left\{\boldsymbol{c}_i \in \mathbb{R}^3 | i = 1, 2, ..., n\right\}$ where $n = D^2$ is the number of coefficients of SH with degree D. The color $\boldsymbol{c}$ of direction $\boldsymbol{d}$ is then computed by summing up all SH basis as $\boldsymbol{c}(\boldsymbol{d}) = \sum_{i=1}^{n} \boldsymbol{c}_i \mathcal{B}_i(\boldsymbol{d})$, where $\mathcal{B}_i$ is the i^{th} SH basis. The final pixel intensity $\boldsymbol{c}$ is calculated by blending n ordered Gaussians overlapping the pixels using the following render function:

$$\boldsymbol{c} = \sum_{i=1}^{n} \boldsymbol{c}_i \alpha_i \prod_{j=1}^{i-1} (1 - \alpha_j) \tag{2}$$

This equation efficiently models the contributions of each Gaussian to the pixel's final appearance, accounting for their transparency and layering order.

Cross-model Feature Aggregation To effectively combine multi-view image features with point-wise geometry information, we implement cross-model attention between two sets of tokens. The original point features $\mathbf{P}$ contain explicit and precise spatial information, which is vital for accurate geometry reconstruction. Conversely, the image token features $\mathbf{F}$ are rich in semantic content, providing crucial contextual details that enhance the overall scene understanding. Cross model fusion allows for the integration of detailed spatial geometry with semantic richness:

$$\begin{aligned} \mathbf{Q} &= \text{Proj}(\mathbf{P}), \\ \mathbf{V}, \mathbf{K} &= \text{Proj}(\mathbf{F}), \\ \mathbf{P} &= \text{softmax}\left(\frac{\mathbf{Q}\mathbf{K}^\top}{\sqrt{d_k}}\right)\mathbf{V} \end{aligned} \tag{3}$$

where $\mathbf{P}$ and $\mathbf{F}$ were normalized with a linear layer before projection.

3.3 Learning Hierarchical Semantics

To facilitate the semantic 3D representation, we augment the anisotropic 3D Gaussians with a learnable feature embedding and rasterize the 3D structure into the 2D image plane by blending Gaussians that overlap with each pixel using a feature rendering function. After obtaining the embeddings on 2D images, we optimize the feature vectors on the 3D Gaussian by minimizing the difference between the rasterized feature map and the feature maps generated by a pre-trained 2D model. Unlike the previous method, Feature-3DGS [13], which requires test-time optimization, we transform the learning of the feature field into a fully learnable process.

3D Semantic Field from 2D Images Indepedent feature maps a pre-trained 2D model is intrinsically view inconsistent as it lack spatial-awareness in the training of 2D model. To elevate multi-view feature embeddings into a coherent 3D feature field for holistic 3D understanding, we introduce a dynamic fusion strategy employing an attention-based correlation module. This module is specifically designed to learn blending weights for each point-based primitive from the input pixel-wise feature embedding. We employ attention blocks as described in Eq.3 to synchronize the latent spaces of semantic image tokens from stereo inputs with point-based networks through a supplementary set of cross-attention layers. The last layer in the dense head of LSeg[66], denoted as $\mathbf{L}$, is utilized for this purpose.

$$\mathcal{L}_{\text{dist}} = 1 - \text{sim}(\mathbf{L}_t, \mathbf{L}_s) = 1 - \frac{\mathbf{L}_t \cdot \mathbf{L}_s}{\|\mathbf{L}_t\| \|\boldsymbol{L}_s\|} \tag{4}$$

This loss function is minimized during training by utilizing rasterized feature maps on new views $\mathbf{L}_s$ and directly inferred feature maps using ground truth images on new views $\mathbf{L}_t$ (LSeg [66]), thereby transferring knowledge and facilitating the lifting of the feature field.

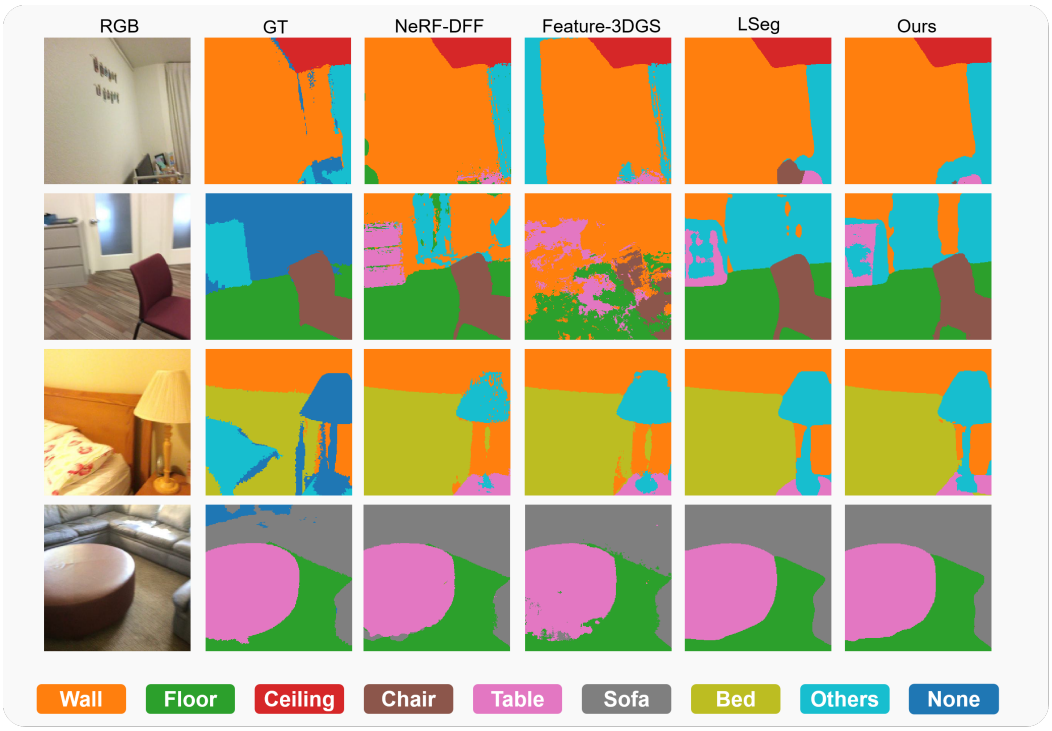

Figure 3: **Language-based 3D Segmentation Comparison**. We visualize the segmentation results in two scenes, and we observe our method perform comparable with NeRF-DFF and Feauture-3DGS. Our results also produce more consistent results cross views than LSeg.

Multi-scale Feature Fusion To enhance model efficiency, we propagate information from $\boldsymbol{F}$ (ViT feature) to $\boldsymbol{P}$ (point feature), which possesses the fewer number of tokens, thereby enabling the selective attention to critical features. We further investigate feature fusion operations across multiple stages, enhancing the effectiveness of information flow while maintaining minimal additional computational cost. See supplementary for detailed design.

3.4 Training Objective

Combining all together, our model can be optimized end-to-end:

$$\mathcal{L} = \underbrace{\left\| \boldsymbol{C}(\boldsymbol{G}, \boldsymbol{d}) - \hat{\boldsymbol{C}} \right\| + \lambda_1 \cdot \text{D-SSIM}(\boldsymbol{C}(\boldsymbol{G}, \boldsymbol{d}), \hat{\boldsymbol{C}})}_{\text{Photometric}} \tag{5}$$

$$+ \lambda_2 \cdot \underbrace{\mathcal{L}_{\text{dist}}(\boldsymbol{L}(\boldsymbol{G}, \boldsymbol{d}), \hat{\boldsymbol{L}})}_{\text{Semantic}} + \sum_{v \in \{1,2\}} \lambda_3 \cdot \underbrace{\mathcal{L}_{\text{depth}}(\boldsymbol{D}_{v,1}, \hat{\boldsymbol{D}}_{v,1})}_{\text{Geometry}} \tag{6}$$

where $\boldsymbol{G}$ denotes represented 3D scene using a set of 3D Gaussians, $\boldsymbol{L}$ and $\hat{\boldsymbol{L}}$ denotes rendered LSeg feature extractor and feature on the target image, $\boldsymbol{d}$ indicates the direction and position at new views. In our methodology, we leverage both photometric loss and semantic loss to supervise the generation of rasterized new views. For geometry prediction, we employ a confidence-weighted depth loss applied to the input views. The parameters λ_1, λ_2, λ_3 are set to 0.25, 0.3, and 1.5, respectively, as determined by grid search.

4 Experiments

4.1 Implementation Details

For our architecture, we employ ViT-Large as the encoder and ViT-Base as the decoder, complemented by a DPT head [30] for pixel-wise geometry regression. We initialize the geometry prediction layers

Table 1: **Quantitative Comparison in 3D Tasks.** We report open-vocabulary segmentation accuracy, depth estimation quality, and novel-view synthesis results. Additionally, our method does not require any preprocessing for these 3D tasks, while achieving performance comparable to other baselines that all require SfM for obtaining camera parameters and poses.

	Reconstruction Time↓		Source View				Target View				
	SfM	Per-Scene	mIoU ↑	Acc.↑	rel ↓	τ ↑	mIoU ↑	Acc.↑	PSNR ↑	SSIM ↑	LPIPS ↓
LSeg	N/A	N/A	0.5278	0.7654	-	-	0.5281	0.7612	-	-	-
NeRF-DFF	20.52s	1min2s	0.4540	0.7173	27.6806	9.6159	0.4037	0.6755	19.8681	0.6650	0.3629
Feature-3DGS	20.52s	18mins36s	0.4453	0.7276	12.9595	21.0732	0.4223	0.7174	24.4998	0.8132	0.2293
pixelSplat	20.52s	0.064s	-	-	-	-	-	-	24.8922	0.8392	0.1641
Ours	0.108s		0.5034	0.7740	3.3853	67.7789	0.5078	0.7686	24.3996	0.8072	0.2506

using DUSR3r [17]. Our framework is structured akin to a U-Net, consisting of eight blocks that alternate between downsampling and upsampling. Cross-model fusion is strategically implemented in the middle and at the first block of the upsampling stage. The entire system is optimized end-to-end using the loss function described in Equation 5. The training of our model contains 100 epochs, leveraging a combined dataset of ScanNet++[67] and Scannet[68], of 1565 scenes. Training is on 8 Nvidia A100 GPU lasts for 3 days. We start with a base learning rate of 1e-4 and incorporate a 10-epoch warm-up period. AdamW is employed as the optimizer for all experiments. Evaluation is conducted on eight unseen datasets from ScanNet, following the methodology established by NeRFingMVS [69]. Additionally, we assess on tasks: language-driven segmentation, novel view synthesis, and multi-view depth prediction across these datasets.

4.2 Semantic 3D Reconstruction

The output of our model is versatile, capable of generating depth maps, novel views, and extracting semantic features from the 3D feature field. We evaluate these capabilities using ScanNet datasets [68] that include all relevant annotations.

Evaluation of Synthesized Images Quality We conducted evaluations on the task of novel view synthesis using our method, NeRF-DFF [12], and Feature-3DGS [13], all of which can predict both RGB and features. Additionally, we compared our results with the state-of-the-art generalizable 3D Gaussian Splatting method, pixelSplat [15], which also generates point-based representations in a feed-forward pass. All these methods require known camera poses prior to training and inference.

As indicated in Table 1, NeRF-DFF and Feature-3DGS tend to overfit on each individual scene, requiring significantly more time than our method, yet performing comparably in terms of output quality. pixelSplat utilizes an Epipolar Transformer, searching along the epipolar line using GT camera parameters to regress Gaussian attributes, resulting in longer inference times. Visualizations in Figure 5 demonstrate that our results are sharper and exhibit fewer artifacts than NeRF-DFF, handle lighting changes more effectively than pixelSplat, and are comparable to Feature-3DGS in performance. Additional visualizations are available in our supplementary materials.

Evaluation of Open-vocabulary Semantic 3D Segmentation The semantic segmentation is evaluated by class-wise intersection over union (mIoU) and average pixel accuracy (mAcc) on novel views as metrics. Following the approach of Feature-3DGS [13], we map thousands of category labels from diverse datasets into a set of common categories, including {Wall, Floor, Ceiling, Chair, Table, Bed, Sofa, Others}. We compare our model against two state-of-the-art 3D baselines with the capacity for generating RGB, semantics and depth on any view: Feature-3DGS [13] and NeRF-DFF [12], which are based on 3D-GS [5] and NeRF [4], respectively. Additionally, the model LSeg [66], used as a 2D open-vocabulary segmenter for feature lifting, is included in our comparisons. We present statistics related to the semantic annotations on eight adopted the ScanNet datasets in Table 1, where LSM demonstrates competitive performance compared to baseline 3D methods that require ground-truth camera parameters and extensive per-scene optimization. The visualized results in Figure 3 illustrate that LSM can produce view-consistent semantic maps. In contrast, the 2D method LSeg yields reasonable segmentation results but lacks cross-view consistency. To validate that LSM learns semantically meaningful features, we visualize the lifted feature field using PCA to reduce the high-dimensional features into three channels [12]. As shown in Figure 4, LSM effectively generates a faithful semantic feature field through feed-forward inference using pair images, without the need for COLMAP for pose precomputation or the time-consuming per-scene optimization required by 3D-GS [13].

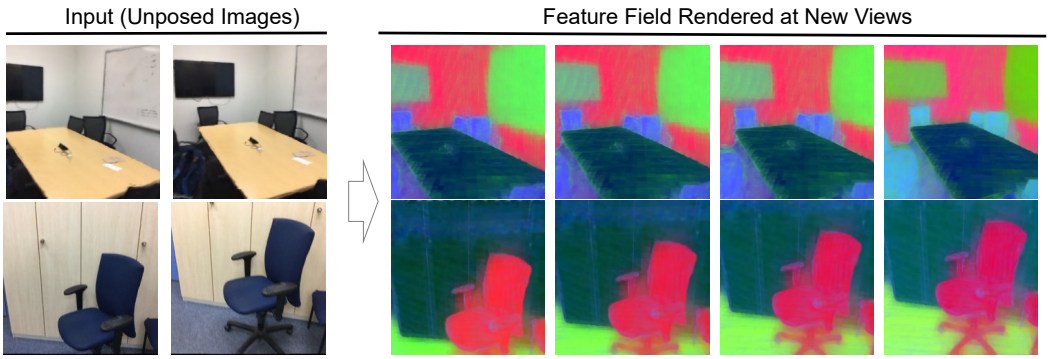

Figure 4: **Visualization of the 3D Feature Field**. We present examples of features rendered from novel viewpoints, illustrating how our method converts 2D features into a consistent 3D, facilitating versatile and efficient segmentation. Visualizations are generated using PCA [70].

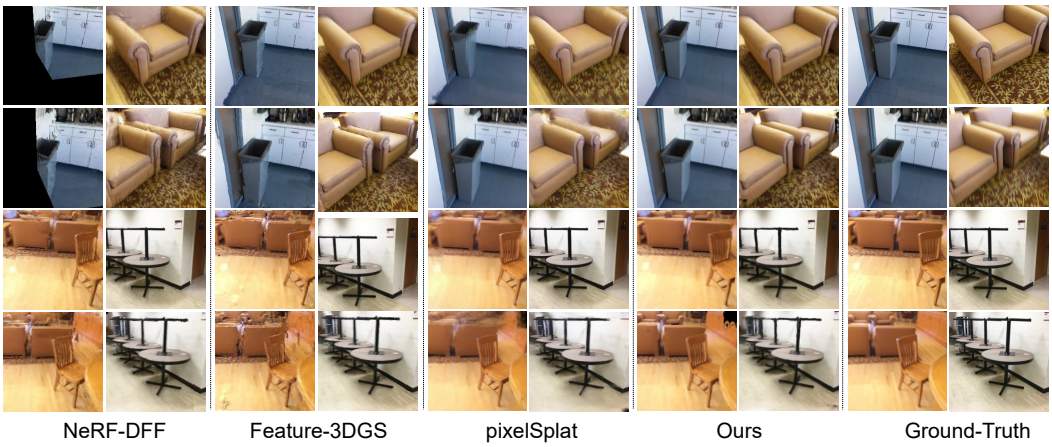

Figure 5: **Novel-View Synthesis (NVS) Comparisons**. We evaluate scene-level reconstruction by comparing our method against those requiring per-scene optimization, such as NeRF-DFF, which can predict both RGB and segmentation, and the generalizable 3D Gaussian Splatting method (pixelSplat). Employing end-to-end training in a data-driven manner, our method achieves visual quality comparable to previous methods while reconstructing the 3D radiance field in a feed-forward pass.

Evaluation of Depth Accuracy We also evaluate the performance of our model on the task of multi-view stereo depth estimation. We utilize the Absolute Relative Error (rel) and Inlier Ratio (τ) with a threshold of 1.03 to assess each scene, similar to DUSt3R [17]. Unlike traditional methods, our approach does not rely on any camera parameters for prediction. Consequently, we align the scene scale between the predictions and the ground truth. Specifically, we normalize the predicted point maps using the median of the predicted depths and similarly normalize the ground truth depths, following procedures established in previous literature [71, 17] to align the two sets of depth maps. We observe in Table. 1 that LSM achieves state-of-the-art accuracy on ScanNet datasets than the per-scene wise methods. Our model is significantly faster than baseline methods, as it only require a forward-pass.

4.3 Ablation Studies

We conduct ablations to validate the effectiveness of the designed framework. Experiments are on the both language-based segmentation and synthesis at novel views. The quantitative results can be views at Table 2.

Cross-Model Feature Aggregation Incorporating the encoder feature from ViT into the hidden layer of the point-aggregation layer (Sec. 3.2) demonstrates that such cross-model information flow significantly benefits the segmentation task, improving the mean Intersection over Union (mIoU) from 0.488 to 0.516 (the first to the second row). It also slightly enhances the rendering quality, with the Peak Signal-to-Noise Ratio (PSNR) increasing from 21.13 to 21.20.

Table 2: **Ablation Study on Our Design Choices.** We evaluate the effectiveness of integrating both cross-view attention and subtraction-based attention, referred to as the baseline configuration. Implementing cross-modal attention to fuse encoder features enhances both the rendering quality of new views and the segmentation accuracy. Additionally, incorporating LSeg features into the fusion process, and multi-scale fusion enhances hierarchical information flow, substantially improving language-based semantic 3D segmentation. Segmentation metrics use LSeg results as ground-truth in this table.

Model	mIoU↑	Acc.↑	PSNR↑	SSIM↑
Baseline	0.4562	0.6940	24.0006	0.7981
+ Fuse Encoder Feat.	0.5410	0.8083	23.6723	0.7876
+ Fuse LSeg Feat.	0.5586	0.8505	23.8585	0.7902
+ Multi-scale Fusion	**0.6042**	**0.8681**	**24.3996**	**0.8072**

Semantic Feature Fusion at Multi-Scale Rather than directly assigning the pixel-aligned feature map from the LSeg model [66] onto the Gaussian, employing cross-model fusion from the LSeg decoder into the middle layer of Point-based aggregation enhances the injection of semantically rich embeddings (0.516 to 0.542). This facilitation improves the rendering of feature maps at novel views. The decoded features validate that the lifted feature field produces higher quality feature maps, with the semantic mIoU improving from 0.542 to 0.599 through multi-scale fusion.

5 Conclusion, Limitation, and Broader Impact

We have introduced the Large Spatial Model, a simple and unified framework for holistic 3D semantic modeling from uncalibrated and unposed images. This framework utilizes cross-view attention to aggregate multi-view cues and employs multi-scale cross-model attention to effectively integrate semantically rich features into a point-based representation. Subtraction-based attention enhances the point-wise regression of diverse point attributes, and an efficient splatting renderer allows for the generation of new views, producing RGB images, depth maps, and encoded features. LSM is highly efficient and capable of conducting end-to-end 3D modeling in real time, thereby supporting various downstream applications.

Although our method significantly accelerates the reconstruction of semantic 3D scenes, it depends on a pre-trained model for feature lifting, consequently requiring increased GPU memory during training, especially when the integrated 2D model contains a large number of parameters. While there are millions of multi-view datasets annotated with depth maps available, the necessity for ground-truth depth maps could restrict its scalability to internet-scale video applications.

Our research enables the efficient reconstruction of 3D digit scene-level and enable the ablity for 3D understanding at real-time. This technology is advantageous for various applications such as AR/VR, navigation and digital twin. However, there is potential for misuse in the 3D assets where the digital assets are spread arbitrarily or lead to privacy leakage of building structure. These risks can be mitigated through watermarking embedded into the 3D assets.

References

[1] Johannes L Schonberger and Jan-Michael Frahm. Structure-from-motion revisited. In *Proceedings of the IEEE conference on computer vision and pattern recognition*, pages 4104–4113, 2016.

[2] Yao Yao, Zixin Luo, Shiwei Li, Tian Fang, and Long Quan. Mvsnet: Depth inference for unstructured multi-view stereo. In *Proceedings of the European conference on computer vision (ECCV)*, pages 767–783, 2018.

[3] Xiaodong Gu, Zhiwen Fan, Siyu Zhu, Zuozhuo Dai, Feitong Tan, and Ping Tan. Cascade cost volume for high-resolution multi-view stereo and stereo matching. In *Proceedings of the IEEE/CVF conference on computer vision and pattern recognition*, pages 2495–2504, 2020.

[4] Ben Mildenhall, Pratul P Srinivasan, Matthew Tancik, Jonathan T Barron, Ravi Ramamoorthi, and Ren Ng. Nerf: Representing scenes as neural radiance fields for view synthesis. *Communications of the ACM*, 65(1):99–106, 2021.

[5] Bernhard Kerbl, Georgios Kopanas, Thomas Leimkühler, and George Drettakis. 3d gaussian splatting for real-time radiance field rendering. *ACM Transactions on Graphics*, 42(4):1–14, 2023.

[6] Zirui Wu, Tianyu Liu, Liyi Luo, Zhide Zhong, Jianteng Chen, Hongmin Xiao, Chao Hou, Haozhe Lou, Yuantao Chen, Runyi Yang, et al. Mars: An instance-aware, modular and realistic simulator for autonomous driving. *arXiv preprint arXiv:2307.15058*, 2023.

[7] William Shen, Ge Yang, Alan Yu, Jansen Wong, Leslie Pack Kaelbling, and Phillip Isola. Distilled feature fields enable few-shot language-guided manipulation. *arXiv preprint arXiv:2308.07931*, 2023.

[8] Luca De Luigi, Damiano Bolognini, Federico Domeniconi, Daniele De Gregorio, Matteo Poggi, and Luigi Di Stefano. Scannerf: a scalable benchmark for neural radiance fields. In *Proceedings of the IEEE/CVF Winter Conference on Applications of Computer Vision*, pages 816–825, 2023.

[9] Tinghui Zhou, Richard Tucker, John Flynn, Graham Fyffe, and Noah Snavely. Stereo magnification: Learning view synthesis using multiplane images. *arXiv preprint arXiv:1805.09817*, 2018.

[10] Jianmei Dai, Zhilong Zhang, Shiwen Mao, and Danpu Liu. A view synthesis-based 360° vr caching system over mec-enabled c-ran. *IEEE Transactions on Circuits and Systems for Video Technology*, 30(10):3843–3855, 2019.

[11] Wenjing Bian, Zirui Wang, Kejie Li, Jia-Wang Bian, and Victor Adrian Prisacariu. Nope-nerf: Optimising neural radiance field with no pose prior. In *Proceedings of the IEEE/CVF Conference on Computer Vision and Pattern Recognition*, pages 4160–4169, 2023.

[12] Sosuke Kobayashi, Eiichi Matsumoto, and Vincent Sitzmann. Decomposing nerf for editing via feature field distillation. *Advances in Neural Information Processing Systems*, 35:23311–23330, 2022.

[13] Shijie Zhou, Haoran Chang, Sicheng Jiang, Zhiwen Fan, Zehao Zhu, Dejia Xu, Pradyumna Chari, Suya You, Zhangyang Wang, and Achuta Kadambi. Feature 3dgs: Supercharging 3d gaussian splatting to enable distilled feature fields. *arXiv preprint arXiv:2312.03203*, 2023.

[14] Peihao Wang, Xuxi Chen, Tianlong Chen, Subhashini Venugopalan, Zhangyang Wang, et al. Is attention all nerf needs? *arXiv preprint arXiv:2207.13298*, 2022.

[15] David Charatan, Sizhe Li, Andrea Tagliasacchi, and Vincent Sitzmann. pixelsplat: 3d gaussian splats from image pairs for scalable generalizable 3d reconstruction. *arXiv preprint arXiv:2312.12337*, 2023.

[16] Qianqian Wang, Zhicheng Wang, Kyle Genova, Pratul P Srinivasan, Howard Zhou, Jonathan T Barron, Ricardo Martin-Brualla, Noah Snavely, and Thomas Funkhouser. Ibrnet: Learning multi-view image-based rendering. In *Proceedings of the IEEE/CVF Conference on Computer Vision and Pattern Recognition*, pages 4690–4699, 2021.

[17] Shuzhe Wang, Vincent Leroy, Yohann Cabon, Boris Chidlovskii, and Jerome Revaud. Dust3r: Geometric 3d vision made easy. *arXiv preprint arXiv:2312.14132*, 2023.

[18] John Flynn, Ivan Neulander, James Philbin, and Noah Snavely. Deepstereo: Learning to predict new views from the world's imagery. In *Proceedings of the IEEE conference on computer vision and pattern recognition*, pages 5515–5524, 2016.

[19] Tinghui Zhou, Shubham Tulsiani, Weilun Sun, Jitendra Malik, and Alexei A Efros. View synthesis by appearance flow. In *Computer Vision–ECCV 2016: 14th European Conference, Amsterdam, The Netherlands, October 11–14, 2016, Proceedings, Part IV 14*, pages 286–301. Springer, 2016.

[20] Jeong Joon Park, Peter Florence, Julian Straub, Richard Newcombe, and Steven Lovegrove. Deepsdf: Learning continuous signed distance functions for shape representation. In *Proceedings of the IEEE/CVF conference on computer vision and pattern recognition*, pages 165–174, 2019.

[21] Songyou Peng, Michael Niemeyer, Lars Mescheder, Marc Pollefeys, and Andreas Geiger. Convolutional occupancy networks. In *Computer Vision–ECCV 2020: 16th European Conference, Glasgow, UK, August 23–28, 2020, Proceedings, Part III 16*, pages 523–540. Springer, 2020.

[22] Zhen Wang, Shijie Zhou, Jeong Joon Park, Despoina Paschalidou, Suya You, Gordon Wetzstein, Leonidas Guibas, and Achuta Kadambi. Alto: Alternating latent topologies for implicit 3d reconstruction. In *Proceedings of the IEEE/CVF Conference on Computer Vision and Pattern Recognition*, pages 259–270, 2023.

[23] Jiahui Huang, Zan Gojcic, Matan Atzmon, Or Litany, Sanja Fidler, and Francis Williams. Neural kernel surface reconstruction. In *Proceedings of the IEEE/CVF Conference on Computer Vision and Pattern Recognition*, pages 4369–4379, 2023.

[24] Guangcong Wang, Peng Wang, Zhaoxi Chen, Wenping Wang, Chen Change Loy, and Ziwei Liu. Perf: Panoramic neural radiance field from a single panorama. *arXiv preprint arXiv:2310.16831*, 2023.

[25] Shijie Zhou, Zhiwen Fan, Dejia Xu, Haoran Chang, Pradyumna Chari, Tejas Bharadwaj, Suya You, Zhangyang Wang, and Achuta Kadambi. Dreamscene360: Unconstrained text-to-3d scene generation with panoramic gaussian splatting. *arXiv preprint arXiv:2404.06903*, 2024.

[26] Dario Pavllo, Jonas Kohler, Thomas Hofmann, and Aurelien Lucchi. Learning generative models of textured 3d meshes from real-world images. In *Proceedings of the IEEE/CVF International Conference on Computer Vision*, pages 13879–13889, 2021.

[27] Dario Pavllo, Graham Spinks, Thomas Hofmann, Marie-Francine Moens, and Aurelien Lucchi. Convolutional generation of textured 3d meshes. *Advances in Neural Information Processing Systems*, 33:870–882, 2020.

[28] Dario Pavllo, David Joseph Tan, Marie-Julie Rakotosaona, and Federico Tombari. Shape, pose, and appearance from a single image via bootstrapped radiance field inversion. In *Proceedings of the IEEE/CVF Conference on Computer Vision and Pattern Recognition*, pages 4391–4401, 2023.

[29] Jia-Wang Bian, Huangying Zhan, Naiyan Wang, Tat-Jun Chin, Chunhua Shen, and Ian Reid. Auto-rectify network for unsupervised indoor depth estimation. *IEEE transactions on pattern analysis and machine intelligence*, 44(12):9802–9813, 2021.

[30] René Ranftl, Alexey Bochkovskiy, and Vladlen Koltun. Vision transformers for dense prediction. In *Proceedings of the IEEE/CVF international conference on computer vision*, pages 12179–12188, 2021.

[31] Wei Yin, Jianming Zhang, Oliver Wang, Simon Niklaus, Simon Chen, Yifan Liu, and Chunhua Shen. Towards accurate reconstruction of 3d scene shape from a single monocular image. *IEEE Transactions on Pattern Analysis and Machine Intelligence*, 45(5):6480–6494, 2022.

[32] Wei Yin, Jianming Zhang, Oliver Wang, Simon Niklaus, Long Mai, Simon Chen, and Chunhua Shen. Learning to recover 3d scene shape from a single image. In *Proceedings of the IEEE/CVF Conference on Computer Vision and Pattern Recognition*, pages 204–213, 2021.

[33] Olivia Wiles, Georgia Gkioxari, Richard Szeliski, and Justin Johnson. Synsin: End-to-end view synthesis from a single image. In *Proceedings of the IEEE/CVF conference on computer vision and pattern recognition*, pages 7467–7477, 2020.

[34] Guangkai Xu, Wei Yin, Hao Chen, Chunhua Shen, Kai Cheng, and Feng Zhao. Frozenrecon: Pose-free 3d scene reconstruction with frozen depth models. In *2023 IEEE/CVF International Conference on Computer Vision (ICCV)*, pages 9276–9286. IEEE, 2023.

[35] Clément Godard, Oisin Mac Aodha, and Gabriel J Brostow. Unsupervised monocular depth estimation with left-right consistency. In *Proceedings of the IEEE conference on computer vision and pattern recognition*, pages 270–279, 2017.

[36] Jaime Spencer, Chris Russell, Simon Hadfield, and Richard Bowden. Kick back & relax: Learning to reconstruct the world by watching slowtv. In *Proceedings of the IEEE/CVF International Conference on Computer Vision*, pages 15768–15779, 2023.

[37] Wei Yin, Chi Zhang, Hao Chen, Zhipeng Cai, Gang Yu, Kaixuan Wang, Xiaozhi Chen, and Chunhua Shen. Metric3d: Towards zero-shot metric 3d prediction from a single image. In *Proceedings of the IEEE/CVF International Conference on Computer Vision*, pages 9043–9053, 2023.

[38] Jonathan T Barron, Ben Mildenhall, Matthew Tancik, Peter Hedman, Ricardo Martin-Brualla, and Pratul P Srinivasan. Mip-nerf: A multiscale representation for anti-aliasing neural radiance fields. In *Proceedings of the IEEE/CVF International Conference on Computer Vision*, pages 5855–5864, 2021.

[39] Thomas Müller, Alex Evans, Christoph Schied, and Alexander Keller. Instant neural graphics primitives with a multiresolution hash encoding. *ACM transactions on graphics (TOG)*, 41(4):1–15, 2022.

[40] Philipp Lindenberger, Paul-Edouard Sarlin, Viktor Larsson, and Marc Pollefeys. Pixel-perfect structure-from-motion with featuremetric refinement. In *Proceedings of the IEEE/CVF international conference on computer vision*, pages 5987–5997, 2021.

[41] Jianglong Ye, Naiyan Wang, and Xiaolong Wang. Featurenerf: Learning generalizable nerfs by distilling foundation models. In *Proceedings of the IEEE/CVF International Conference on Computer Vision*, pages 8962–8973, 2023.

[42] Stefano Gasperini, Mohammad-Ali Nikouei Mahani, Alvaro Marcos-Ramiro, Nassir Navab, and Federico Tombari. Panoster: End-to-end panoptic segmentation of lidar point clouds. *IEEE Robotics and Automation Letters*, 6(2):3216–3223, 2021.

[43] Zixiang Zhou, Yang Zhang, and Hassan Foroosh. Panoptic-polarnet: Proposal-free lidar point cloud panoptic segmentation. In *Proceedings of the IEEE/CVF Conference on Computer Vision and Pattern Recognition*, pages 13194–13203, 2021.

[44] Kshitij Sirohi, Rohit Mohan, Daniel Büscher, Wolfram Burgard, and Abhinav Valada. Efficientlps: Efficient lidar panoptic segmentation. *IEEE Transactions on Robotics*, 38(3):1894–1914, 2021.

[45] Lyne Tchapmi, Christopher Choy, Iro Armeni, JunYoung Gwak, and Silvio Savarese. Segcloud: Semantic segmentation of 3d point clouds. In *2017 International Conference on 3D Vision (3DV)*, pages 537–547, 2017.

[46] Loic Landrieu and Martin Simonovsky. Large-scale point cloud semantic segmentation with superpoint graphs. In *Proceedings of the IEEE Conference on Computer Vision and Pattern Recognition (CVPR)*, June 2018.

[47] Antoni Rosinol, Arjun Gupta, Marcus Abate, Jingnan Shi, and Luca Carlone. 3d dynamic scene graphs: Actionable spatial perception with places, objects, and humans. *arXiv preprint arXiv:2002.06289*, 2020.

[48] Gaku Narita, Takashi Seno, Tomoya Ishikawa, and Yohsuke Kaji. Panopticfusion: Online volumetric semantic mapping at the level of stuff and things. In *2019 IEEE/RSJ International Conference on Intelligent Robots and Systems (IROS)*, pages 4205–4212. IEEE, 2019.

[49] Nicolas Carion, Francisco Massa, Gabriel Synnaeve, Nicolas Usunier, Alexander Kirillov, and Sergey Zagoruyko. End-to-end object detection with transformers. In *European conference on computer vision*, pages 213–229. Springer, 2020.

[50] Sara Fridovich-Keil, Alex Yu, Matthew Tancik, Qinhong Chen, Benjamin Recht, and Angjoo Kanazawa. Plenoxels: Radiance fields without neural networks. In *Proceedings of the IEEE/CVF Conference on Computer Vision and Pattern Recognition*, pages 5501–5510, 2022.

[51] Peng Wang, Lingjie Liu, Yuan Liu, Christian Theobalt, Taku Komura, and Wenping Wang. Neus: Learning neural implicit surfaces by volume rendering for multi-view reconstruction. *arXiv preprint arXiv:2106.10689*, 2021.

[52] Michael Oechsle, Songyou Peng, and Andreas Geiger. Unisurf: Unifying neural implicit surfaces and radiance fields for multi-view reconstruction. In *Proceedings of the IEEE/CVF International Conference on Computer Vision*, pages 5589–5599, 2021.

[53] Dejan Azinović, Ricardo Martin-Brualla, Dan B Goldman, Matthias Nießner, and Justus Thies. Neural rgb-d surface reconstruction. In *Proceedings of the IEEE/CVF Conference on Computer Vision and Pattern Recognition*, pages 6290–6301, 2022.

[54] Shuaifeng Zhi, Tristan Laidlow, Stefan Leutenegger, and Andrew J Davison. In-place scene labelling and understanding with implicit scene representation. In *Proceedings of the IEEE/CVF International Conference on Computer Vision*, pages 15838–15847, 2021.

[55] Vadim Tschernezki, Iro Laina, Diane Larlus, and Andrea Vedaldi. Neural feature fusion fields: 3d distillation of self-supervised 2d image representations. In *2022 International Conference on 3D Vision (3DV)*, pages 443–453. IEEE, 2022.

[56] Suhani Vora, Noha Radwan, Klaus Greff, Henning Meyer, Kyle Genova, Mehdi SM Sajjadi, Etienne Pot, Andrea Tagliasacchi, and Daniel Duckworth. Nesf: Neural semantic fields for generalizable semantic segmentation of 3d scenes. *arXiv preprint arXiv:2111.13260*, 2021.

[57] Xiao Fu, Shangzhan Zhang, Tianrun Chen, Yichong Lu, Lanyun Zhu, Xiaowei Zhou, Andreas Geiger, and Yiyi Liao. Panoptic nerf: 3d-to-2d label transfer for panoptic urban scene segmentation. In *2022 International Conference on 3D Vision (3DV)*, pages 1–11. IEEE, 2022.

[58] Abhijit Kundu, Kyle Genova, Xiaoqi Yin, Alireza Fathi, Caroline Pantofaru, Leonidas J Guibas, Andrea Tagliasacchi, Frank Dellaert, and Thomas Funkhouser. Panoptic neural fields: A semantic object-aware neural scene representation. In *Proceedings of the IEEE/CVF Conference on Computer Vision and Pattern Recognition*, pages 12871–12881, 2022.

[59] Bing Wang, Lu Chen, and Bo Yang. Dm-nerf: 3d scene geometry decomposition and manipulation from 2d images. *arXiv preprint arXiv:2208.07227*, 2022.

[60] Alexey Dosovitskiy, Lucas Beyer, Alexander Kolesnikov, Dirk Weissenborn, Xiaohua Zhai, Thomas Unterthiner, Mostafa Dehghani, Matthias Minderer, Georg Heigold, Sylvain Gelly, et al. An image is worth 16x16 words: Transformers for image recognition at scale. *arXiv preprint arXiv:2010.11929*, 2020.

[61] Jiaming Sun, Zehong Shen, Yuang Wang, Hujun Bao, and Xiaowei Zhou. Loftr: Detector-free local feature matching with transformers. In *Proceedings of the IEEE/CVF conference on computer vision and pattern recognition*, pages 8922–8931, 2021.

[62] Philippe Weinzaepfel, Vincent Leroy, Thomas Lucas, Romain Brégier, Yohann Cabon, Vaibhav Arora, Leonid Antsfeld, Boris Chidlovskii, Gabriela Csurka, and Jérôme Revaud. Croco: Self-supervised pre-training for 3d vision tasks by cross-view completion. *Advances in Neural Information Processing Systems*, 35:3502–3516, 2022.

[63] Rui Chen, Songfang Han, Jing Xu, and Hao Su. Point-based multi-view stereo network. In *Proceedings of the IEEE/CVF international conference on computer vision*, pages 1538–1547, 2019.

[64] Meng-Hao Guo, Jun-Xiong Cai, Zheng-Ning Liu, Tai-Jiang Mu, Ralph R Martin, and Shi-Min Hu. Pct: Point cloud transformer. *Computational Visual Media*, 7:187–199, 2021.

[65] Hengshuang Zhao, Li Jiang, Jiaya Jia, Philip HS Torr, and Vladlen Koltun. Point transformer. In *Proceedings of the IEEE/CVF international conference on computer vision*, pages 16259–16268, 2021.

[66] Boyi Li, Kilian Q Weinberger, Serge Belongie, Vladlen Koltun, and René Ranftl. Language-driven semantic segmentation. *arXiv preprint arXiv:2201.03546*, 2022.

[67] Chandan Yeshwanth, Yueh-Cheng Liu, Matthias Nießner, and Angela Dai. Scannet++: A high-fidelity dataset of 3d indoor scenes. In *Proceedings of the IEEE/CVF International Conference on Computer Vision*, pages 12–22, 2023.

[68] Angela Dai, Angel X Chang, Manolis Savva, Maciej Halber, Thomas Funkhouser, and Matthias Nießner. Scannet: Richly-annotated 3d reconstructions of indoor scenes. In *Proceedings of the IEEE conference on computer vision and pattern recognition*, pages 5828–5839, 2017.

[69] Yi Wei, Shaohui Liu, Yongming Rao, Wang Zhao, Jiwen Lu, and Jie Zhou. Nerfingmvs: Guided optimization of neural radiance fields for indoor multi-view stereo. In *Proceedings of the IEEE/CVF International Conference on Computer Vision*, pages 5610–5619, 2021.

[70] Fabian Pedregosa, Gaël Varoquaux, Alexandre Gramfort, Vincent Michel, Bertrand Thirion, Olivier Grisel, Mathieu Blondel, Peter Prettenhofer, Ron Weiss, Vincent Dubourg, et al. Scikit-learn: Machine learning in python. *the Journal of machine Learning research*, 12:2825–2830, 2011.

[71] Philipp Schröppel, Jan Bechtold, Artemij Amiranashvili, and Thomas Brox. A benchmark and a baseline for robust multi-view depth estimation. In *2022 International Conference on 3D Vision (3DV)*, pages 637–645. IEEE, 2022.